CHAPTER 4

Discussion

4.1 Initiation of growth fault and mass transport complex

Most common type of the growth faults takes into account ductile lithologies (i.e. salt, overpressured shale) to form detachment later (Back and Morley, 2016). Their initiation and development is commonly associated with differential loading triggered by rapid accumulation of overlying overburden, or gravity driven process controlled by migration of a delta front (e.g. Niger Delta; Rouby et al., 2011; Colombian Caribbean Margin; Alfaro and Holz, 2014). The north-south trending growth faults documented from the northern Taranaki Basin faults sole out in the intra-Mangaa claystone and cause structural rollover in the underlying Mangaa sand unit. The growth faults are typically compensated along the upslope extension by a down-slope compression (fold and thrusts). However, the fault initiation mechanism in this study area is distinct from typical growth faults model as discussed previously. For example, they show very little of downslope compressional domain of small toe thrusts and do not ramp up from the detachment surface following the fault-propagation fold model. In addition, there is no obvious loading trigger for the faults as they initiate at the base of slope of the Giant Foresets Formation and no evidence of any mobile shale being present (Morley and Naghadeh, 2016). Morley and Naghadeh (2016) proposed that the loss of porosity, due to lateral fluid migration caused by the GFF loading, can be the triggering mechanism for fault initiation. Loading by the overlying GFF forced the overpressured fluid to migrate basinward, followed by the failure at the base of slope occurred as consequence of this overpressured fluid (Fig. 4.1). In this case, the fluid was likely to be expelled during the active progradation of the highstand systems tracts during the Early Pliocene (HST1). The loading of the prograding sequences affected the footwall area, not the hanging wall. In Figure 4.1 the effects of progradational sediment loading of a zone around location X about 1 km deep in the subsurface is considered. Loading produced a small increase in the differential stress at the detachment level (Fig. 4.1B1 path a), but if progradation of the Giant Foresets Formation drove transient overpressured fluidsbasinwards due to loading then failure at the base of the slope triggered by the increase in pore fluid pressure (Fig. 4.1B1 path b).

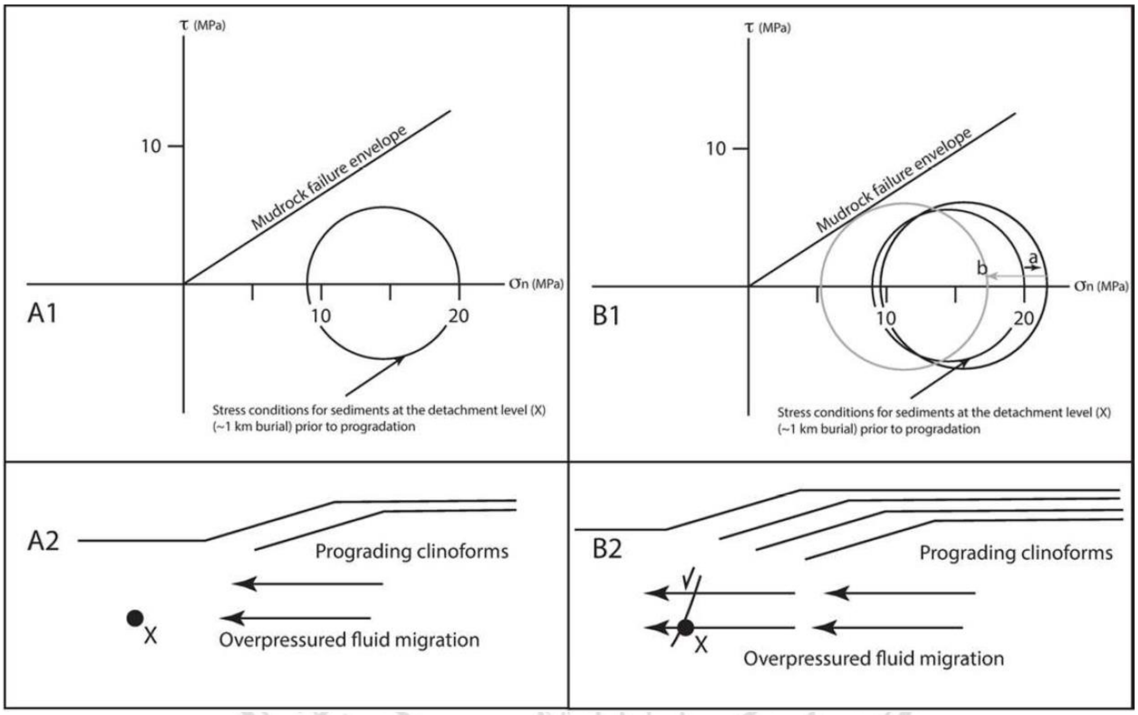

Figure 4.1: Model for the development of a listric normal fault at the base of prograding sequence. A) Stress at location X prior to loading, and arrival of overpressured fluids. B) Stress state at location X after initial loading, and arrival of laterally expelled overpressured fluids. (Source: Morley and Naghadeh, 2016).

Mass transport complexes (MTC) are prevalent within the growth fault sections. Most of the MTC volume is localized within the growth fault and is recognized from its low amplitude, chaotic reflections due to its downslope transportation. Although the existence of basal groove marks can directly record the translation of the MTC body across the basal surface (Wang et al., 2014), this feature cannot be identified from the seismic data within the study area. However, other kinematic indicators as previously discussed in chapter 3, reveal that the transport direction of the MTC is from east to west. Presence of headscarp in the eastern part, compressional ridge internal small-scale toe thrusts in the west and other kinematic indicators such as rotational block can help constrain the transport direction of the MTC with greater confidence.

The occurrence of the MTC within this study was under much speculation whether the MTC fill in the depression was controlled by the fault, or it helped triggering the fault. From the 3D seismic, the MTC is observed to scour some portions of the Karewa fault and underlying H3 (base syn-kinematic sequence of the Karewa fault). The location of the headscarp indicates that the MTC did not move very far, and is also restricted by the antithetic fault in the north (Fig.3.4). From this observation, the MTC was likely to occur during the late stage of the Karewa fault activity (Late-Pliocene).

The triggering mechanism of the MTC in this study was illustrated in Figure 4.2. In this case, the local destabilization of the sediment packages can be considered as the main triggering mechanism. The destabilization probably caused by overpressured fluids escaping along the fault (Fig.4.2A). The destabilized surface is observed as a listric, concave upward feature, which reflects the initial movement of this MTC (Fig.3.4C), followed by translation of the MTC volume along this surface (Fig.4.2B). The MTC is then ramped up and formed contractional features in order to compensate the slumping into the growth fault section. Probably a similar event affected the Mangaa Fault too, which also shows an MTC in its growth section. This is an example of highly unusual MTC that is longer in the strike-direction than it is in the transport direction with the dimension of about 25×5 km^2 (Fig.3.10). In the later stage, the MTC is buried by the overlying sequences (Fig.4.2C). Ultimately, this MTC causes a low relief slope to accommodate the progradational event and allow the thick succession of the Giant Foresets Formation to form.

This MTC can be classified as the ‘‘frontally emergent’’ type based on Frey’s classification (Frey-Martinez, 2006), and also as “slump deposit” based on its sedimentary structures and seismic features observed (Moscardelli et al. 2006) e.g. compressional ridge, rotational block, contorted layers (Fig.3.4). The MTC may have evolved into a debris flow and turbidity current if there is sufficient water content (Nicole, 2009). This scenario may explain the reason that the MTC has travelled for about 3-4 km from the growth fault section in some parts of the study area (Fig.3.5 and 4.2B).

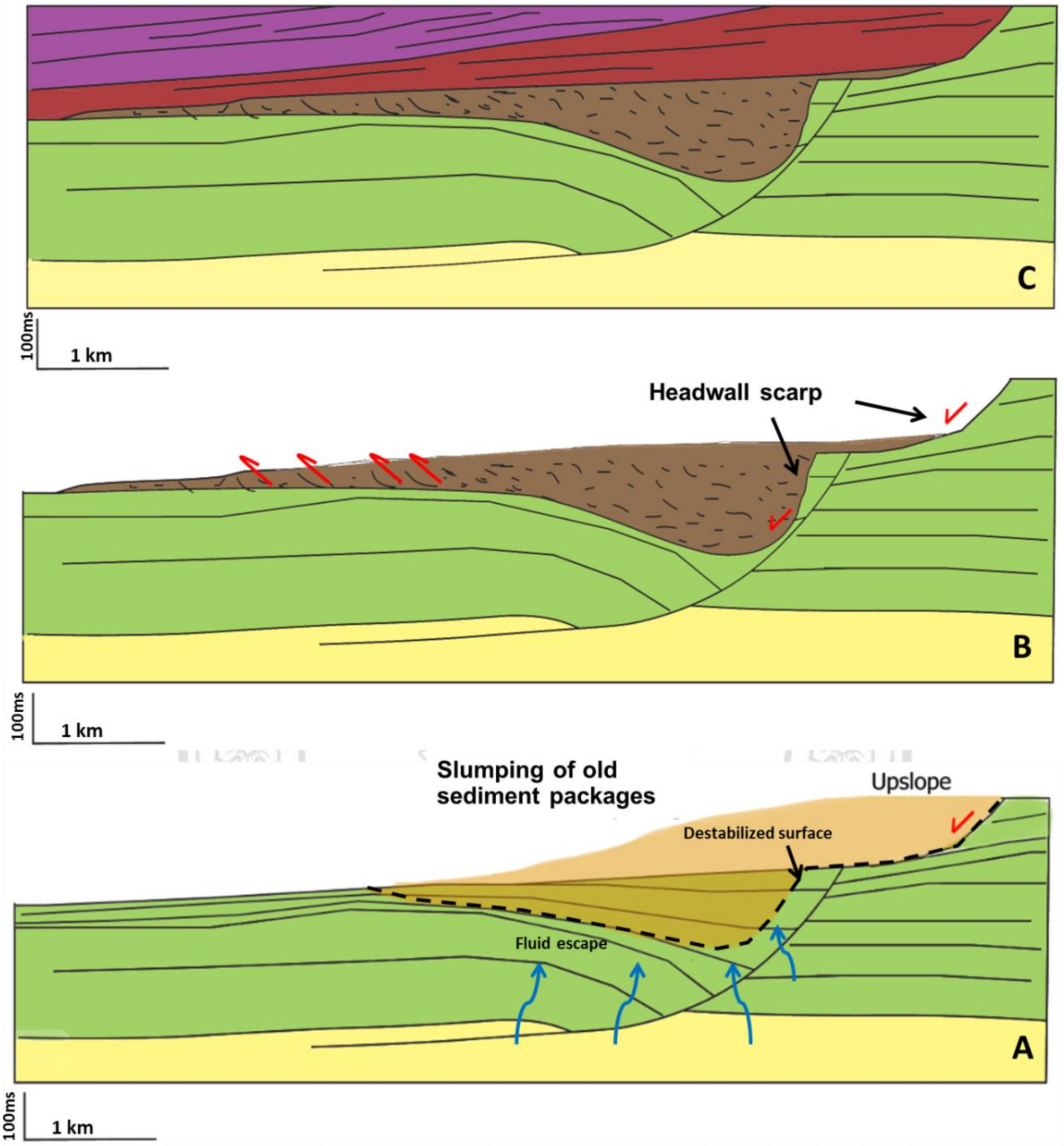

Figure 4.2: Schematic diagram illustrates development of the MTC within the study area A) initial stage prior to movement, B) translation and toe region creation of the MTC along the destabilized surface caused by fluid escape, C) Burial of the MTC by subsequent sedimentation during the Pliocene.

4.2: Depositional History of the Prograding Sequences

Detail examination on a set of 2D and 3D seismic data reveals the depositional history and elements of the prograding sequence within the study area known informally as the Giant Foresets Formation (GFF). The age of the GFF has been constrained by biostratigraphy using New Zealand stages (Hollis et al., 2010) ranging from Opoitian (5.2-3.5 Ma or latest Miocene-Early Pliocene) at the base and Late Nukumaruan at the top (1.8-0.33 Ma or Pleistocene) (Hansen and Kamp, 2006). The GFF documented in this study area is relatively younger in age ranging from Nukumaruan (2.35 Ma or Late Pliocene) Ma at the base to Recent Castlecliffian (< 1.3 Ma) at the top based on the lithology information reported in Karewa-1 well (Conoco, 2013). The maximum thickness of the Giant Foresets Formations reported up to 2000m thick recorded within the Northern Graben and the NW of the western platform (Hansen and Kamp, 2002). However, the GFF in the study area accumulated a total thickness ranging from 600-1200m in the north to 400-1400m in the south of the study area. This is indicates late progradational phase recorded within the study area with the modern shelf continue to migrate basinward to the west.

The central part of the study area where the GFF are bounded by a fault from eastern side and topographic high in the west, displays straighten-out clinoform geometry. While in the southern part, where there are two growth faults present, the clinoforms display bold geometry with increased sediment thickness. This southward augmented thickness in clinoforms can be attributed to the accommodation space previously created by the Mangaa fault located in the south. Figure 4.3 shows the depositional history of the progradational sequences in the study area using P95-118 seismic line located in the south. The relationship of the depositional trend to the relative sea-level oscillation driving the accommodation generation has been demonstrated as well. Figure 4.4 shows correlation of base level curve with the published sea levels dataset from the last 5 million years (Pliocene-Holocene) (Hansen, 2016). The diagram show sea level based on proxy datasets from various observations (e.g. radio isotopes from ice, sediment cores, coral growth, tree rings, etc.) in this data show the transition of the Pliocene to the Pleistocene, there is a pronounced change in behaviour of the curve. The marker to constrain the base level curve of this study is the top boundary of Falling Stage Systems Tract (FSST) which is 1.77 Ma according to the Karewa-1 well report. In this case, this marker was match to the Hansen curve and the age to constrain the beginning and the end of the curve from the study is approximated in relative age.

The matching of sea-level curve within this study suggests a good correlation to the Hansen curve. Overall, the Hansen sea level curve has been dynamic throughout the Neogene, but the long term trend indicates that the sea level dropped to level about 50-80 m below modern sea-level during 2.2-1.4 Ma. This concurs with lowstands sea level observed within the study area. The highstand sea-level during 2.6-2.2 also has a good matching. However, during the last 800 Ka (Pleistocene) the Hansen curve display extreme oscillation of sea level, especially in the terminal Pleistocene from about 600 Ka to the LGM (Last Glacial Maximum). Therefore, the second highstand event is more difficult to match interpreted base-level curve into this interval.

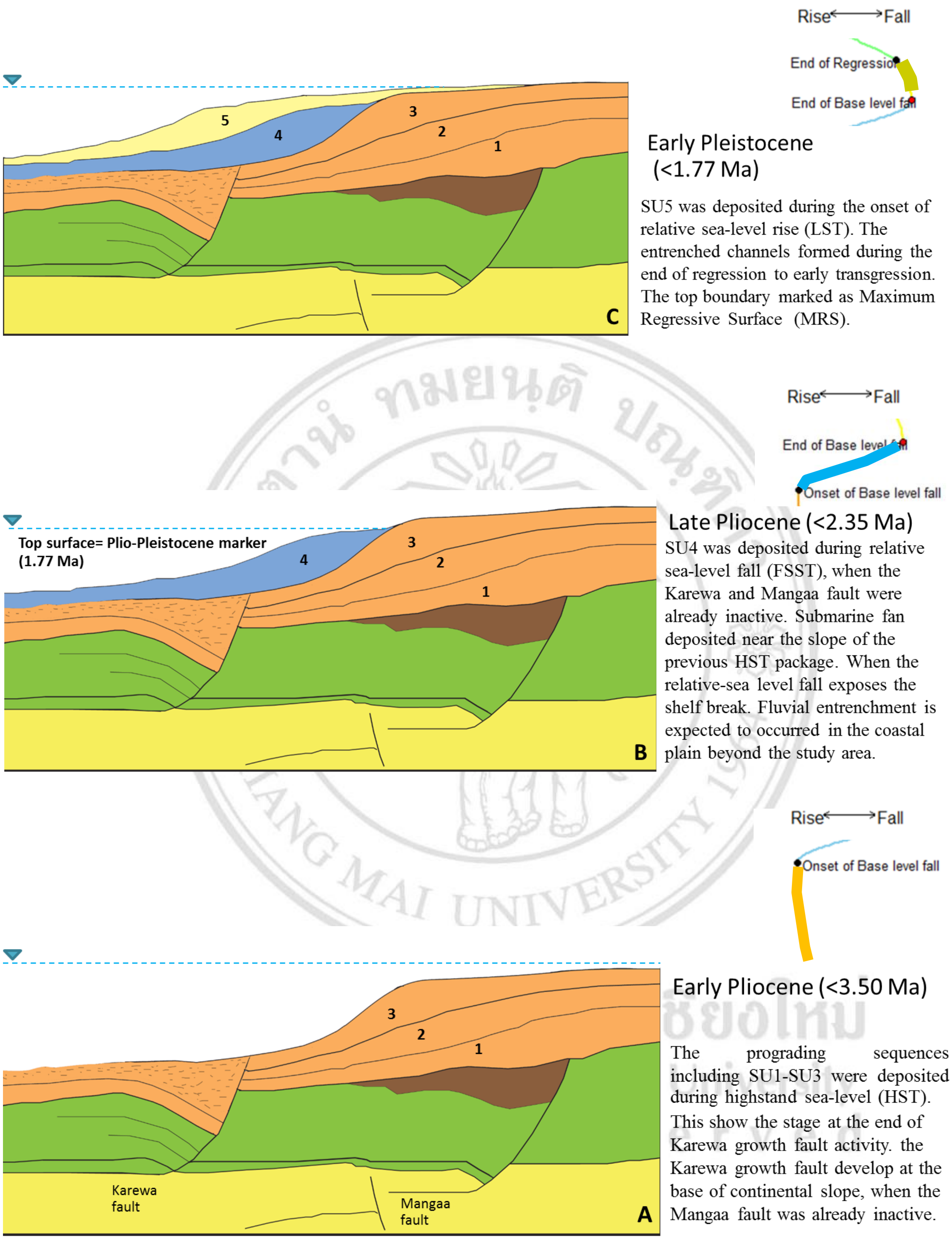

Figure 4.3: Conceptual model shows the depositional history of the prograding sequences (A-C) in the study area and the timing of the post growth-faults depositional trend associated with the relative sea-level changes through time.

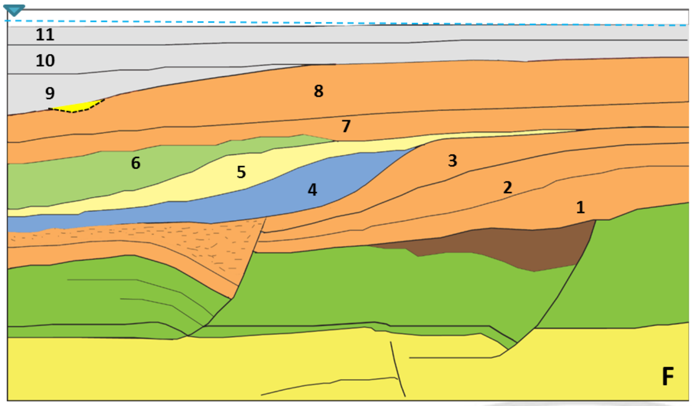

Late Pleistocene-Recent

In the late stage of HST deposit and channel incision, the sediment keep funnel into the study area and deposit parallel to the present-day seafloor. The sediment package included SU9-SU11 which likely to comprise pelagic sediment and probably some terrigenous sediments transported by mega-channels

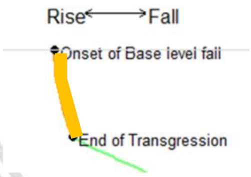

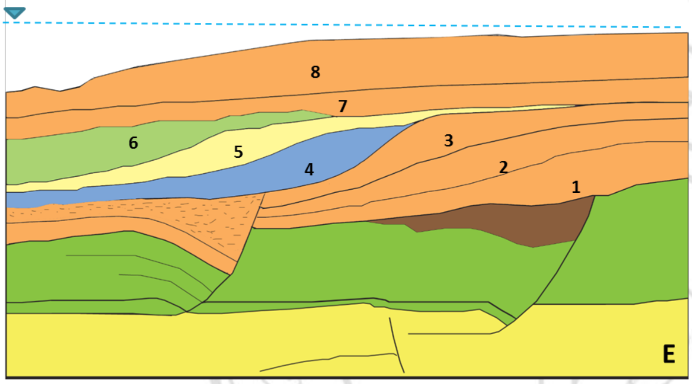

Late Pleistocene

The sequences deposited during highstand including SU7 and SU8. The sea-level at this stage is steadily and the sediment rates outpaced sea-level rise. The slope id relatively low suggesting the degradation phase of the prograding sequence. In the late stage of HST deposit, there was incision by mega-channels during Late Pleistocene

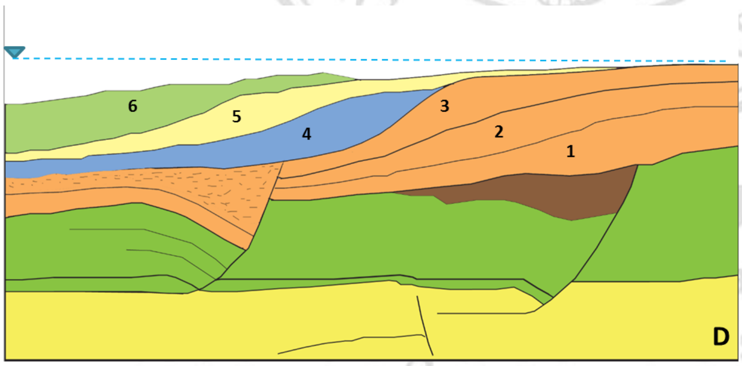

Early Pleistocene (<1.77 Ma)

SU6 was deposited during the transgressive (TST), where the sea-level increased and forced back-stepping of sediments to deposit shelfward. The top boundary marked as Maximum Transgressive Surface (MFS).

Figure 4.3 (Con.) : Conceptual model shows the depositional history of the prograding sequences (D-F) in the study area and the timing of the post growth-faults depositional trend associated with the relative sea-level changes through time.

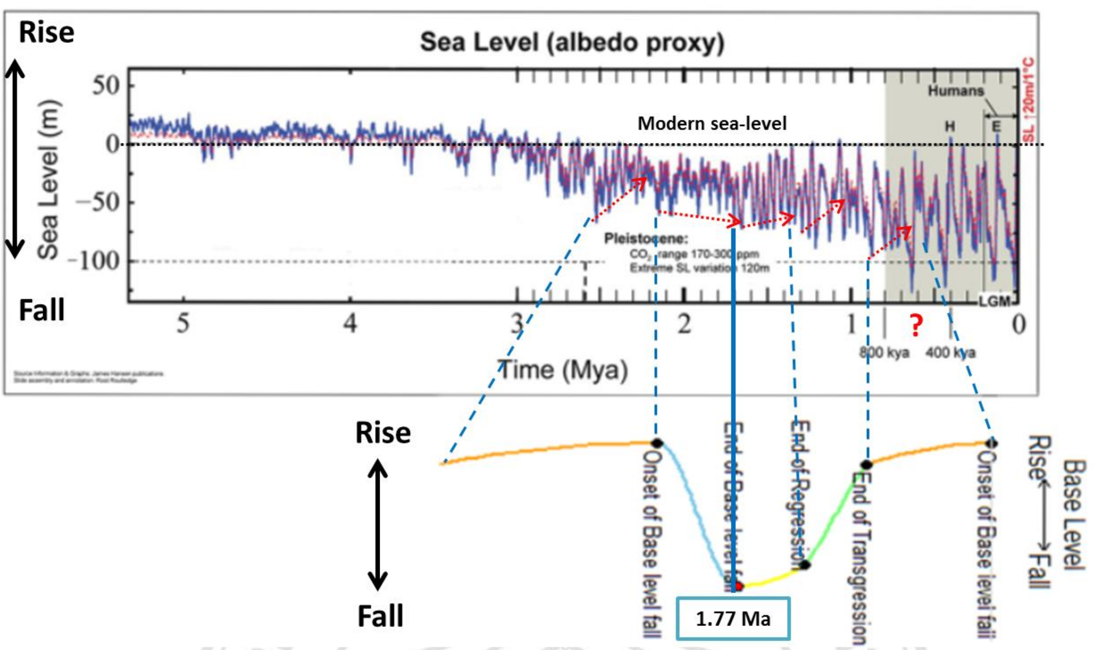

Figure 4.4: Correlation of the base-level curve of this study with the Hansen sea-level curve during the last 5 million years. (Modified from Root Routledge, created from source information from Jame Hansen publications)

Mapping of the key bounding horizons and systems tracts interpretation reveal that the succession of the GFF was deposited during an extended period of the highstand sea-level (i.e. two cycle of highstand). The base-level curves show that the progradational sequence was deposited in the full cycle of seal-level fall and rise during the Pliocene-Pleistocene (Fig.3.25 and 3.26).

Fig.4.3A shows that the first high stand systems tract (HST) package deposited in the late stage of the Karewa growth fault, followed by the falling stage systems tract (FSST) deposits. The top boundary of the SU4 marks Plio-Pleistocene age and can be interpreted as a maximum regressive surface (MRS). This interpretation suggests that during Pliocene, sediments were deposited in the through relative sea-level fall (Fig.4.3B). It is reasonable to consider that the shelf of the previous HST might have been exposed and underwent fluvial entrenchment during this stage. If so, there should be records of fluvial entrenchment along the eastern shelf. Unfortunately, there are inadequate seismic data in the east to confirm this assumption and also the 3D seismic data only encompasses the slope portion of the FSST, and no data for HST toward east.

However, during the early Pleistocene the relative sea-level started rising up again, resulting the creation of accommodation space to deposit the sediments for Low stand systems Tract (LST) (Fig.4.3C). The top boundary is interpreted as a Maximum Regressive Surface (MRS) which recorded the event from the end of regression to early transgression. Fortunately, the 3D seismic located in the slope portion reveal the entrenched channels and slump features related to this systems tract. The depositions (SU6) during the Trasgressive Systems Tract (TST) exhibit backstepping of sediments shelfward (Fig.4.3D). The sea-level was increasing rapidly and marked the top boundary as a Maximum Transgressive Surface (MFS).

Until the Late Pleistocene-Recent, the sediment succession have been deposited in a relatively low gradient slope, which suggests rate of sediment influx outpaced rates of sea-level rise, Because the sequences display more aggradational stacking pattern as the shelf edge moving slightly westward (Fig.4.3E). There are Submarine channels observed on seismic section. The phantom horizons extracted within this second HST package, applied with the RGB-spectral decomposition shows more sinuous channel geometry with obvious “Y” shaped tributary channels. The differences in term of sinuosity, width/depth ratio and temporal scale can be used as significant indicators to support the interpretation of depositional history influenced by relative sea-level changes. The younger HST package was observed to be eroded by the mega-channels in the southern part of the study area and they are transported from the SE. This erosion event, caused by the mega-channels can be observed more clearly in the Wheeler diagram. Finally, the recent package of SU9-SU10 (Fig.4.3F) is likely to make up of pelagic sediments and probably the terrigenous sediment filling up until the present-day seafloor.